Applied Radiation and Isotopes 225 (2025) 111979

Contents lists available at ScienceDirect

Applied Radiation and Isotopes

journal homepage: www.elsevier.com/locate/apradiso

Monte Carlo dosimetry of silver-111 in simplified cell geometries in the framework of the ISOLPHARM project

A. Donzella [a,b], A. Leso [c,d,*], A. Arzenton [e,f], G. Bonomi [a,b], S. Bortolussi [g,b], D. Chen [e,f], S. Corradetti [c], M. Lunardon [e,f], E. Mariotti [h,i], E. Reniero [e], D. Serafini [c,h], G.S. Valli [e], L. Zangrando [f], A. Zenoni [a], A. Andrighetto [c]

[a] Department of Mechanical and Industrial Engineering, University of Brescia, Via Branze 38, 25123 Brescia, Italy
[b] Pavia Division, National Institute for Nuclear Physics, Via A. Bassi 6, 27100 Pavia, Italy
[c] Legnaro National Laboratories, National Institute for Nuclear Physics, INFN-LNL, Viale dell' Università 2, 35020 Legnaro, Italy
[d] Department of Physics and Earth Sciences, University of Ferrara, Via G. Saragat, 1, 44122 Ferrara, Italy
[e] Department of Physics and Astronomy, University of Padova, Via F. Marzolo 8, 35131 Padova, Italy
[f] Padova Division, National Institute for Nuclear Physics, Via F. Marzolo 8, 35131 Padova, Italy
[g] Department of Nuclear and Theoretical Physics, University of Pavia, Via A. Bassi 6, 27100 Pavia, Italy
[h] Department of Physical Sciences, Earth and Environment, University of Siena, Via Roma 56, 53100 Siena, Italy
[i] Pisa Division, National Institute for Nuclear Physics, Largo B. Pontecorvo 3, 56127 Pisa, Italy

ARTICLE INFO

Keywords:
Nuclear physics applications
Medical applications
Dosimetry
Monte Carlo method
Silver-111
ISOLPHARM
TRT

ABSTRACT

The ISOLPHARM project of the INFN aims to study the properties of the ^{111}Ag β^- emitter as a promising core for novel radiopharmaceuticals. ^{111}Ag will be produced at the SPES facility of the Legnaro National Laboratories, with high specific activity and remarkable yields, exploiting the ISOL technique. This work presents Monte Carlo dosimetry calculations at cellular level to assess the therapeutic potential of ^{111}Ag within the ADMIRAL project. Using the formalism introduced by the MIRD, S-values are calculated for a biological cell exposed to different scenarios of activity distributions of ^{111}Ag. The results of dosimetry calculations performed with GEANT4, MCNP6 and PHITS Monte Carlo codes are presented and discussed, showing a good mutual agreement and also with the MIRDcell values. These results will be used within the ISOLPHARM project for the planning of in-vitro experiments in 2D cell cultures and 3D tissue-mimicking scaffolds.

1. Introduction

In recent years, Targeted Radionuclide Therapy (TRT) is becoming a promising strategy for cancer therapy, alongside the External Beam Radiation Therapy (EBRT) (Brosch-Lenz et al., 2023; Sun et al., 2023). The use of unconventional theranostic radionuclides significantly enhances the potential and application of TRT, while also driving fundamental research in this field. TRT relies on radiopharmaceuticals – chemical compounds incorporating a radioactive isotope – designed to deliver therapeutic and diagnostic effects through their specific decay properties. For the development of high-quality radiopharmaceuticals, radionuclides with high radionuclidic purity and, preferably, in a carrier-free form, are essential. These features ensure preparations with high purity and molar activity (Am), which is particularly critical when designing receptor-based radiotracers. In fact, maintaining high Am prevents the saturation of target receptors, thereby optimizing imaging and therapeutic efficacy (Srivastava and Mausner, 2014).

A promising approach for the production of high-purity radioisotopes for medical applications, alternative to traditional production routes in nuclear reactors or accelerators, is based on the Isotope Separation On-Line (ISOL) technique (dos Santos Augusto et al., 2014). This technique, that dates back to the early '50s, is exploited in the context of ISOLPHARM (ISOL technique for radioPHARMaceuticals), a multidisciplinary research project aiming to produce innovative radioisotopes for nuclear medicine at the SPES facility (Selective Production of Exotic Species) of the Italian INFN-LNL (National Institute for Nuclear Physics – Legnaro National Laboratories) (Andrighetto et al., 2019; Ballan et al., 2020).

SPES is equipped with a cyclotron that can accelerate a proton beam towards a primary production target, inducing nuclear reactions (e.g., proton-induced fission on ^{238}U nuclei if a fissile uranium carbide target is used Monetti et al., 2015). Due to the high temperature of the target (about 2000 °C), the radioactive nuclear fragments produced

* Corresponding author at: Department of Physics and Earth Sciences, University of Ferrara, Via G. Saragat, 1, 44122 Ferrara, Italy.
E-mail address: aurora.leso@lnl.infn.it (A. Leso).

https://doi.org/10.1016/j.apradiso.2025.111979
Received 3 March 2025; Received in revised form 5 June 2025; Accepted 5 June 2025
Available online 11 July 2025

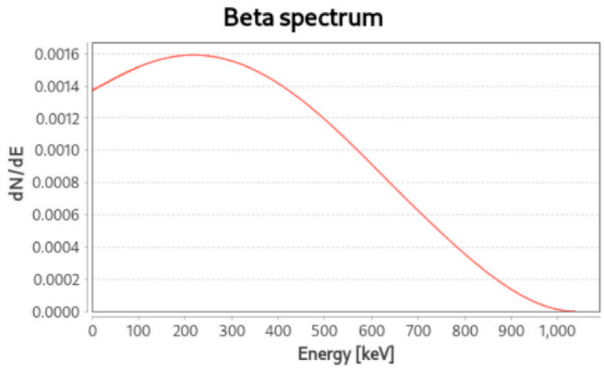

Fig. 1. β^- decay spectrum of ^{111}Ag from the IAEA nuclear database (International Atomic Energy Agency (IAEA), 2025).

diffuse towards an ion source, where a part of them is ionized and then extracted at low energy (Centofante et al., 2021; Lilli et al., 2023). Then, the so-produced Radioactive Ion Beam (RIB) is transported along a dedicated beam line and reaches a mass spectrometer (the Wien filter) that selects only isotopes with a specific mass (Monetti et al., 2024). At the exit of the Wien filter, the isobaric ion beam is collected onto a secondary target system. After chemical purification, the radioisotope of interest is finally ready to be extracted and used for labeling proper radiopharmaceutical preparations, to be tested by means of preclinical in-vitro and in-vivo studies (Ballan et al., 2021). Due to the mass separation step, the ISOL technique allows beams with high radionuclidic purity and high specific activity to be produced at the SPES facility. Some of these radionuclides are particularly interesting as a core for innovative radiopharmaceuticals and have not been explored so far due to their tricky production with current methods, which makes them poorly available.

Using a uranium carbide matrix as primary production target, very intense neutron-rich RIBs will be produced at SPES in the coming years (Corradetti et al., 2021; Andrighetto et al., 2023). Among them, several radioisotopes that exhibit β^- decay are promising in TRT because of their decay characteristics (i.e., half-life, radiation type and released energy) (Corradetti and Andrighetto, 2020).

The latest experiment supported by the ISOLPHARM collaboration, ADMIRAL (Advanced Dosimetry Methods and In-vitro Radiobiology of Ag-111 Labeled radiopharmaceuticals,2023–2025), has the main purpose of investigating the diagnostic and therapeutic properties of the ^{111}Ag radioisotope (Serafini et al., 2025). ^{111}Ag is a promising β^- emitter with a half-life of 7.45 d. Its main β^- emission (I_β = 92%) has an average energy of 360.4 keV, suitable for cancer therapy (the spectrum is shown in Fig. 1). Furthermore, it emits two γ rays of medium energy (E_γ = 245.4 keV, I_γ = 1.2%; E_γ = 342.1 keV, I_γ = 6.7%). For these reasons, it potentially allows for simultaneous therapy and monitoring in-vivo of the delivered dose by associated Single Photon Emission Computed Tomography (SPECT) imaging (Tosato and Asti, 2023). These 'theranostic' properties resemble those of ^{177}Lu, which was recently approved by the U.S. Food and Drug Administration (Brosch-Lenz et al., 2023; Tosato et al., 2023), and ^{186}Re, which has been recently tested in phase I/II clinical trials (Denis-Bacelar et al., 2017). Since with the ISOL technique the isotopic contaminants of silver are removed by the mass separation, ^{111}Ag will be produced at SPES with high specific activity and good yields (Monetti et al., 2015), up to 2 Ci in target after 5 days of operation (Corradetti and Andrighetto, 2020).

Within ADMIRAL, the therapeutic potential of ^{111}Ag is assessed by means of cell survival experiments, exploiting 2D cell cultures and 3D tissue-mimicking scaffolds to obtain realistic cell cultures in dynamic conditions (Arzenton, 2023). To correlate the biological effect measured in cells with the dose absorbed due to ^{111}Ag, Monte Carlo calculations are employed for a detailed dosimetry. In fact, the capacity of ^{111}Ag to cause lethal damage depends on the amount of radioisotope taken up by the cells and on their shapes and volumes. The computed absorbed dose is then used as input for specific cell population models to evaluate the cell survival fraction, based on several assumptions about DNA damage and repair mechanisms. Finally, the outcome of these models can be compared with the experimental data (Arzenton, 2023). Furthermore, simulations of the cytoplasmic environment with specific tools, such as Geant4-DNA (Incerti et al., 2010), are performed to directly predict the physicochemical processes leading to direct and indirect radiation damage on the DNA (Leso, 2023).

In the present work, several Monte Carlo dosimetry calculations at cellular level are discussed and compared, exploiting the formalism of the cellular S-values introduced by the Committee on Medical Internal Radiation Dose (MIRD) of the U.S. Society of Nuclear Medicine and Molecular Imaging (SNMMI) (Bolch et al., 2009).

The paper is organized as follows. Section 2 illustrates the motivations of the study and describes the method used in the Monte Carlo cell dosimetry simulations, based on the S-value formalism. The calculation tools used in the study are discussed, detailing the physical models and the options implemented in each of them. In Section 3, the results of the calculations are presented for each of the different scenarios supposed within the study; in particular, different spatial distributions of the ^{111}Ag activity, with respect to the target cell, are considered and discussed. Finally, in Section 4 conclusions are drawn.

2. Calculation of cellular absorbed dose

To evaluate the effects of the ^{111}Ag radioisotope on cell survival in the context of TRT, several in-vitro tests will be performed in the framework of the ADMIRAL project, exploiting monolayer 2D cultures as well as 3D scaffolds obtained from bioprinting (Doctor et al., 2020). These radiobiological experimental data must be related to the absorbed dose at cell level. The Monte Carlo method allows to calculate the absorbed dose released in a biological cell model exposed to different activity distributions of ^{111}Ag.

Absorbed dose calculations have been performed using different tools for Monte Carlo simulation: Geant4 version 11.1 (Agostinelli et al., 2003; Allison et al., 2006, 2016), MCNP6 version 1.0 (Goorley et al., 2013) and PHITS version 3.32 (Sato et al., 2024). They are able to simulate the transport and interaction with the physical media for several particles, including electrons and photons, in a user-defined geometry. Specific information, such as the absorbed dose distribution in assigned volumes, can be requested by the code user.

2.1. Monte Carlo method

Internal radiation dosimetry calculations are performed using the S-value formalism introduced by the MIRD (Bolch et al., 2009). This scheme allows for the evaluation of the absorbed dose at the cellular level when a radiopharmaceutical preparation is administered to a patient. It considers the case of target organs, tissues belonging to an organ, voxelized tissues from SPECT or PET images and individual cells.

When the dose assessment concerns a single cell isolated or immersed in a tissue, as is the case considered in the present study, it can be assumed that both the source and the target masses remain constant in time (Brosch-Lenz et al., 2023). Consequently, the dose $D(r_T, T_D)$ (measured in Gy) absorbed by the cellular target r_T, integrated over the irradiation period T_D, can be written as:

$$D(r_T, T_D) = \sum_{r_S} \tilde{A}(r_S, T_D) S(r_T \longleftarrow r_S), \quad (1)$$

where $\tilde{A}(r_S, T_D)$, expressed in Bq s, is the time-integrated activity in the source tissue r_S. The proportionality constant $S(r_T \longleftarrow r_S)$, called the *S-value*, represents the mean dose rate absorbed in r_T per unit

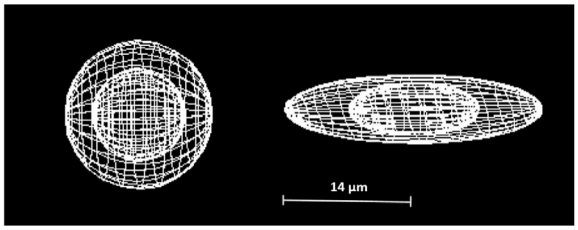

Fig. 2. Spherical and ellipsoidal cell geometries used in this study (Reniero, 2023).

administered activity in r_S. The S-value, depending on the specific radionuclide, is measured in Gy/(Bq s).

The absorbed dose estimated with these assumptions depends on the anatomic model considered. In the case of the present study, the S-value in Eq. (1) is calculated for a biological cell exposed to different activity distributions of ^{111}Ag. The Monte Carlo geometry model considers simplified spherical and ellipsoidal cell structures, with dimensions similar to those generally found in the literature for this type of study (see Fig. 2) (Sakata et al., 2020; Shin et al., 2021). The spherical cell consists of two concentric spheres of radii 8 μm (corresponding to the external membrane) and 5 μm (corresponding to the cell nucleus). The ellipsoidal cell has the same volume as the spherical one: external membrane with major semi-axis of 14 μm and minor semi-axis of 2.5 μm, nucleus with major semi-axis of 7 μm and minor semi-axis of 2.5 μm, coincident with the membrane one.

In a further analysis, it is studied how the S-values change when altering the shape of the cell, in particular its eccentricity. Starting from the spherical shape, the minor semi-axis of the cell is reduced from 8 μm to 2.5 μm in 11 steps, keeping the volume of the cell constant. The nucleus is flattened until its minor semi-axis is equal to the one of the cell.

The material of the cell (membrane, cytoplasm and nucleus) as well as the external biological environment, modeled as a sphere large enough to contain all the cellular structures, are supposed to be water-equivalent (density $\rho = 1\,\mathrm{g/cm^3}$).

The source energy is sampled on the decay spectrum of ^{111}Ag in its stable ^{111}Cd isobar. Since ^{111}Ag is a 100% β^- emitter, for each disintegration event of the ^{111}Ag radioisotope, the source emits one β^- electron. The generation volume depends on the spatial distribution of the source r_S, which in turn depends on the particular biological model chosen to evaluate the efficacy of the drug. The study considers three different scenarios:

- self-absorbed dose, when the source cell is the same as the target cell and the electron is emitted from the cellular membrane, from the cytoplasm or from the whole cell (in the eccentricity study, the electron is also emitted from the nucleus);
- cross-absorbed dose, when the source cell is moved at increasing distance from the target cell and the electron is emitted from the membrane or by the whole cell;
- environmental dose, when the source electron is coming from the space external to the target cell.

As in these calculations the cellular regions are characterized by uniform density, in the Monte Carlo model the events are homogeneously distributed in the source volume and the flight directions are isotropic. To build the membrane volume, a thickness of 0.01 μm is attributed to the membrane body. The assessment of $S(r_T \longleftarrow r_S)$ is performed calculating the energy deposition in the target volume: either the whole cell or its nucleus. The energy is then converted in average dose per unit of cumulated activity (dose per source event in the Monte Carlo calculation).

Table 1
Comparison of S-Values in mGy/(Bq s) with nucleus target and spherical cell geometry. Monte Carlo statistical uncertainties are lower than 1%.

Source	Geant4	MCNP6	PHITS	MIRDcell
Membrane	0.071	0.069	0.066	0.064
Cytoplasm	0.115	0.111	0.106	0.118
Cell	0.183	0.172	0.165	0.168

2.2. Monte Carlo simulation setting

Due to the continuous slowing-down of electrons during their path, following electrons in each single collision requires long calculation times. To optimize the transport strategy in relation to the geometrical dimensions of the model and to the energy range involved, different physics models and libraries are utilized in Geant4, MCNP6 and PHITS.

In Geant4, the `G4EmStandardPhysics_option3` library is implemented, with a cut-off range of 0.1 mm for the electrons and 1 mm for the photons (Arzenton, 2024). Within this physics list, the `G4RadioactiveDecayPhysics` library containing the decay spectrum of ^{111}Ag radioisotope is activated.

The MCNP6 algorithm used for electron energies above 100 keV is a Condensed-History transport (Schaart et al., 2002). It consists of gathering the effects of many individual collisions inside a definite material in single energy steps and sub-steps, driving the estep option (estep=100 instead of 3 as calculated by default in water (Antoni and Bourgois, 2017)). A Single-Event transport is set for electron energies below 100 keV (instead of 1 keV as by default) and until 1 keV, enabling the ENDF/B VI.8 cross section database (EPRDATA12) (Grady Hughes, 2014). The differences in the results of the absorbed dose calculated in the case of self-absorbed dose, using this optimized electron transport method, compared to those calculated by the default method, are of the order of 3%, with an increase in computation time by a factor of 3. Concerning the photons, the cut-off energy is 1 keV as for electrons.

In PHITS, the default cut-off energy of 1 keV for electrons and 100 keV for photons is adopted. The negs=1 option is used in the Parameters section for the transport of electrons and photons based on the EGS5 algorithm (Electron Gamma Shower Version 5) (Hirayama et al., 2005). The DECDC nuclear decay database is implemented to generate the decay spectrum of ^{111}Ag (Endo et al., 2005). No time evolution is considered (dtime option=0).

The use of several codes with different models and libraries may imply some discrepancies in the simulation results. For this reason, a systematic deviation is expected.

3. Results and comparison between codes

3.1. Self-absorbed dose

Fig. 3 reports the results of the S-values calculated with the three Monte Carlo codes for the case of self-absorbed dose from an activity distribution of the ^{111}Ag radioisotope on a spherical cell. The S-values are compared to those provided by MIRDcell, a software tool widely used in the medical field for internal radiation dosimetry (Vaziri et al., 2014; Katugampola et al., 2022).

The source is located on the cell membrane, in the cytoplasm and on the whole cell, while the energy deposition is scored in the cell nucleus and over the whole cell. The S-values are in mGy/(Bq s). Each simulation consists in the emission of 10^7 source events and takes about one hour of running on a single PC (Intel Core i7-7700 CPU, 3.60 GHz and 16 GB RAM) for all Monte Carlo codes, sufficient to keep the statistical error below 1%. In Tables 1 and 2 the S-values calculated under all the conditions shown in Fig. 3 are reported.

In general, the dose depends on where the electron source is located, given the geometries and dimensions involved in the study. When the β^- decays occur in the whole cell (plot (c) in Fig. 3), the absorbed dose

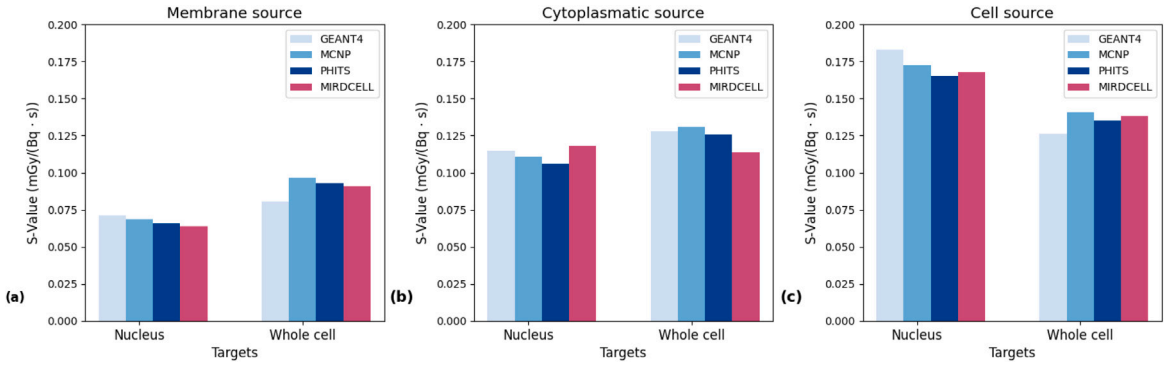

Fig. 3. S-values in the nucleus and over the whole cell for an activity distribution of ^{111}Ag radioisotope in the spherical cell geometry. Source tissue on the membrane (a), in the cytoplasm (b) and on the whole cell (c). Monte Carlo statistical uncertainties are lower than 1%.

Table 2
Comparison of S-Values in mGy/(Bq s) with whole cell target and spherical cell geometry. Monte Carlo statistical uncertainties are lower than 1%.

Source	Geant4	MCNP6	PHITS	MIRDcell
Membrane	0.083	0.097	0.093	0.091
Cytoplasm	0.128	0.131	0.125	0.114
Cell	0.126	0.141	0.135	0.138

Table 3
Comparison of S-Values in mGy/(Bq s) with nucleus target and ellipsoidal cell geometry. Monte Carlo statistical uncertainties are lower than 1%.

Source	Geant4	MCNP6	PHITS
Membrane	0.085	0.082	0.075
Cytoplasm	0.075	0.073	0.067
Cell	0.149	0.138	0.128

Table 4
Comparison of S-Values in mGy/(Bq s) with whole cell target and ellipsoidal cell geometry. Monte Carlo statistical uncertainties are lower than 1%.

Source	Geant4	MCNP6	PHITS
Membrane	0.072	0.084	0.078
Cytoplasm	0.091	0.107	0.099
Cell	0.098	0.114	0.106

in the spherical nucleus is 23% higher than in the whole cell (calculated from the average of the values in the last row of Tables 1 and 2). The opposite result occurs in the other cases where the source is distributed on the membrane or in the cytoplasm (plots (a) and (b) in Fig. 3). The difference in these cases is 25% for the membrane and 11% for the cytoplasm (first and second rows of Tables 1 and 2).

Let us look now instead at the S-value on the whole cell (four right blocks in each plot). When the electron activity is localized on the cell membrane (a), the S-value results lower than if the activity is distributed more internally, by 27% if in the cytoplasm (b) and 33% if in the whole cell (c). This is due to the fact that the membrane is on the boundary of the cell and the emission of electrons is isotropic, so many of them do not enter the cell.

Regarding the comparison among the three developed Monte Carlo codes, Fig. 3 shows that MCNP6 provides the highest S-value results over the whole cell for each activity distribution. The same is true with Geant4 for S-values to the nucleus. Tables 1 and 2 evidence that the difference between the S-values from all Monte Carlo codes and the MIRDcell ones is generally a few percent and in the worst case less than 15%, in agreement with the literature (Cai et al., 2017). This result allows for a validation of the model calculations developed in the present study.

In Fig. 4 a comparison is presented between the results of the self-absorbed dose for a spherical cell and for an ellipsoidal cell. All the S-values are calculated with Geant4. Tables 3 and 4 report the S-values

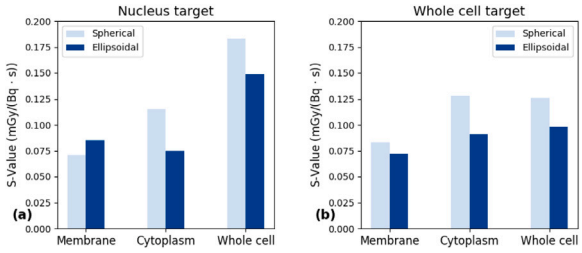

Fig. 4. Comparison of Geant4 calculated S-values with target in the nucleus (a) and in the whole cell (b), for a spherical cell and for an ellipsoidal cell. Monte Carlo statistical uncertainties are lower than 1%.

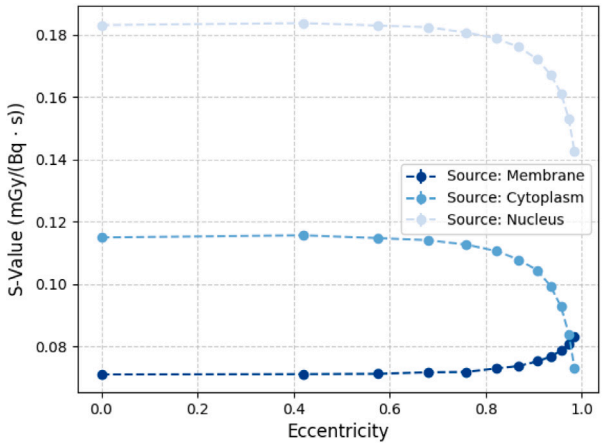

Fig. 5. Behavior of S-values in the nucleus versus eccentricity, for an activity distribution on the membrane (dark blue), in the cytoplasm (medium blue) and in the nucleus (light blue). Monte Carlo statistical uncertainties are lower than 1%.

calculated with the three Monte Carlo codes in the different cases of source and target bodies, for an ellipsoidal cell geometry. In the case of the ellipsoidal cell, the dose absorbed is generally lower than that calculated for the spherical cell, except than the dose absorbed by the nucleus for source distribution on the membrane.

This fact is well evidenced by the behavior of the S-value curves in the nucleus as a function of eccentricity, shown in Fig. 5. In this study, the electron is emitted from the membrane, the cytoplasm and the nucleus instead of by the whole cell, to emphasize how the dose is affected by the shape of the cell when the source is placed more internally. If the activity is on the membrane, the S-value in the nucleus is initially a factor 1.6 lower than placing the source in the cytoplasm, and a factor 2.6 lower for the source in the nucleus. However, unlike the case of activity in the cytoplasm or in the nucleus, the S-value

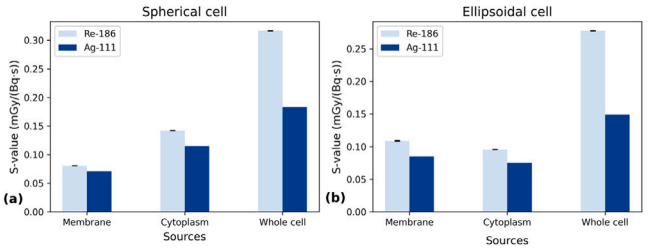

Fig. 6. Comparison of GEANT4 calculated S-values with spherical cell geometry (a) and ellipsoidal cell geometry (b) for ^{111}Ag and ^{186}Re considering the cell nucleus as target.

increases with eccentricity. This behavior is due to the progressive thinning of the cytoplasm near the two poles touching the nucleus, which places the membrane globally closer to the nucleus. Instead, considering the activity sources in the cytoplasm and in the nucleus, it is evident from Fig. 5 that the S-value decreases with ϵ. This is again due to the geometry: if the source is distributed in the cytoplasm, the more the cell is flattened, the more the particles radiated in the outer part of the cytoplasm are not able to reach the nucleus. On the other hand, if the source is in the nucleus, with increased eccentricity the outermost particles escape from the nucleus after a shorter path, releasing a smaller portion of their energy in this region.

Concerning the ^{111}Ag radioisotope at these intracellular distances, the dose deposited in the cellular target medium is mainly due to electron interactions. Here, the photon dose is about 10^4 times lower than the electron dose; the two contributions become comparable only about 4.5 mm from the source, since a tiny fraction of the electrons emitted reaches this distance (see Fig. 2.9 of Arzenton, 2024).

Finally, in order to present a comparison between the biological effects of ^{111}Ag and a pure β^- emitter already used for clinical purposes, GEANT4 simulations were performed using a ^{186}Re source. The same geometrical settings for targets and sources have been used and the resulting S-value comparison between the two radionuclides is presented in Fig. 6 (with the cell nucleus as target). As one can see, when the source is located either on the membrane or within the cytoplasm, the two radionuclides give similar results, with differences within 28%. On the other hand, when the source is distributed in the whole cell,^{186}Re shows higher S-values. This behavior can be explained considering the emission characteristics of the two radionuclides: as a matter of fact, compared to ^{111}Ag,^{186}Re emits a greater amount of low-energy, short-range Auger and conversion electrons (International Atomic Energy Agency (IAEA), 2025). When the source is distributed in the whole cell, some of these electrons are emitted within or near the nucleus, probably becoming responsible for the observed higher energy deposition in the target. However, since drug internalization in the cell nucleus is usually difficult, distributions of the two nuclides on the membrane or in the cytoplasm can be expected to cause a similar DNA damage yield per activity unit. Clearly, when developing a therapeutic plan, one must take into account that ^{186}Re has a shorter half-life ($\sim$ 3.7 d), which means a higher specific activity.

3.2. Cross-absorbed dose

In evaluating the cross-absorbed dose, the target cell is initially positioned adjacent to the emitting cell. For the ellipsoidal geometry, the cells are in contact in the plane of the major semi-axes (28 μm distance between the centers). Then, the target cell is moved up to a distance of 2–3 mm from the source cell, corresponding to hundreds of radii or mayor axes (for the ellipsoidal cell). Simulations are performed with GEANT4 and PHITS, for activity distributions on both the membrane and the whole cell. However, when the distance is much larger than the cell radius, the cell shape and the source location become negligible, as the two cells behave as if they were point-like.

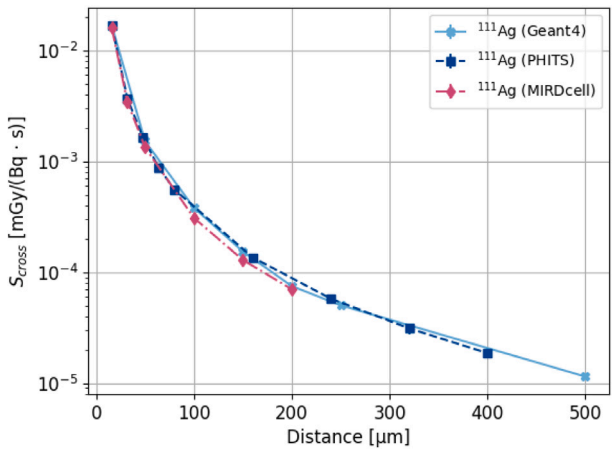

Fig. 7. Behavior of S-values in whole cell versus distance between spherical source and target cells, for an activity distribution of ^{111}Ag on the membrane. Monte Carlo statistical uncertainties amount up to 10% at distances around 400–500 μm.

In Fig. 7, the S-values simulated in the whole cell are compared to those of MIRDcell, for a membrane activity distribution on a spherical cell. The points on the curves are calculated until 500 μm distance with 10^7 events generated for each run, corresponding to a maximum statistical error below 10%. The differences between the simulated and MIRDcell S-values range from about 1% to 20%, in accordance with the literature (Cai et al., 2017). The S-value decreases by 90% or more already within 50 μm distance between centers (equivalent to 3 diameters), while at 150 μm the residual value is less than 1%. At a distance of 500 μm between centers, the S-value decreases by a factor of 10^3 compared to the contact case. This behavior has been observed for all the activity distributions. For the ellipsoidal case, instead, the required distance to decrease the S-value on the whole cell below 1% is between 250 μm and 300 μm (depending on the activity distribution), which is about 100 μm more with respect to the spherical case.

Finally, looking at the cross-absorbed dose for a spherical cell, a clear decrease in S-values is observed after a few millimeters. This is due to the decay properties of the β^- ^{111}Ag radioisotope and to the decreasing solid angle. As a matter of fact, electrons of 360.4 keV, the average energy distribution of the β^- spectrum, have a range in water of approximately 1.1 mm (National Institute of Standards and Technology (NIST), 2025).

3.3. Environmental dose

The last task carried out in this study is the calculation of the dose absorbed by the cell when the radiopharmaceutical is placed in the external environment. The study considers a spherical environment with an increasing radius of up to 3 mm, enough for the S-value to reach a plateau beyond which larger source distributions no longer affect the cell dose intake. This is shown in Fig. 8, where the simulations are performed with GEANT4 and PHITS for a spherical cell. Also, it can be seen that the S-value points on the two curves are compatible until some percent even at large environment radii. For an ellipsoidal cell, the differences of S-values, with respect to the ones calculated for the spherical cell, are negligible after 2–3 cell radii (as in the previous case of the cross-absorbed dose).

To maintain the statistical error below a few percent, the number of events in the Monte Carlo is determined considering that the event/volume ratio outside the cell should remain constant, starting from 10^6 with radius 0.1 mm and up to $5 \cdot 10^8$ with radius 3 mm. As a consequence, the unit of measurement of the S-values is normalized per source events and per unit of volume: mGy/(Bq s) μm^3. The simulations with large radii take about 1 day of running on a single PC.

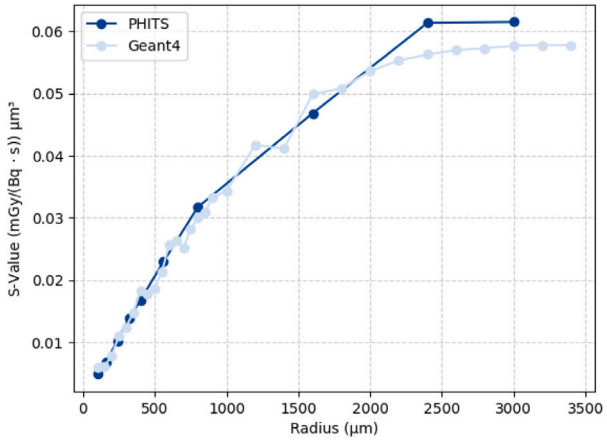

Fig. 8. Environmental S-values calculated with GEANT4 and PHITS for a spherical cell. Monte Carlo statistical uncertainties are under a few percent at all distances.

As underlined in Section 3.1, up to about 3 mm the energy released in the cell by a ^{111}Ag distribution in the surrounding environment comes mainly from β^- decay, whose contribution becomes less important than the decay photons only at distances higher than about 4–5 mm. In conclusion, the plateau value, which is around 0.06 mGy/(Bq s) µm^3, can be used in the context of in-vitro experiments to account for the concentration of activity outside the cells, that is, the one coming from the non-internalized radiopharmaceutical. This scenario is particularly reliable in the first rounds of radiobiological experiments, where the radioisotope is administered without any carrier, which prevents an effective uptake of ^{111}Ag in the cells.

4. Summary and conclusions

The Italian ADMIRAL project of INFN-LNL assesses the therapeutic potential of the ^{111}Ag radioisotope, a promising β^- emitter for cancer therapy. Dosimetry calculations are performed with three different tools for Monte Carlo simulation: GEANT4, MCNP6 and PHITS. The S-values formalism suggested by the American Committee on the Medical Internal Radiation Dose (MIRD) is exploited by considering a biological cell exposed to various activity distributions of ^{111}Ag. These calculations will be useful to plan and understand the outcomes of in-vitro cell survival experiments exploiting monolayer 2D cell cultures as well as 3D scaffolds.

From the calculations performed in the case of self-absorbed dose, it is deduced that all three Monte Carlo codes give S-values globally in agreement with each other, and also with the MIRDcell values, within 15%. This result is probably due to the systematic differences between the models and the libraries used by the codes; nevertheless, it is consistent with the data reported in the literature and allows for a validation of the Monte Carlo model developed in the present study.

Dealing with self-absorption, the dose depends on the geometry of both the source and target volumes. In general, for a spherical cell, the dose deposited on the entire cell or in its nucleus is lower if the electron source is distributed more externally. This behavior is not very different from what occurs in the case of an ellipsoidal cell. However, in the latter case, the absorption of the electron energy strongly depends on the thinning of the nucleus. In addition, a comparison between ^{111}Ag and ^{186}Re, a radionuclide currently undergoing clinical trials, revealed that the S-values originating from their β^- radiations are very similar, in the most likely cases where the drug is internalized in the cytoplasm or bound to the cell membrane.

In the case of the cross-absorbed dose, the S-value decreases to about 1% of its initial value when the distance from the source cell reaches a few hundred microns, due to the β^- decay properties of ^{111}Ag. Similarly, the external environment affects the dose imparted to the cell at distances up to approximately 3 mm, where the γ-ray contribution is still negligible with respect to the β^-. These features open the possibility of employing the radioisotope in the treatment of small to medium-sized tumors, without affecting nearby healthy tissues.

CRediT authorship contribution statement

A. Donzella: Writing – original draft, Validation, Software, Methodology, Investigation, Formal analysis, Data curation, Conceptualization. **A. Leso:** Writing – original draft, Visualization, Validation, Software, Methodology, Investigation, Formal analysis, Data curation, Conceptualization. **A. Arzenton:** Writing – original draft, Visualization, Validation, Software, Methodology, Investigation, Formal analysis, Data curation, Conceptualization. **G. Bonomi:** Writing – review & editing, Supervision. **S. Bortolussi:** Writing – review & editing, Supervision, Formal analysis, Conceptualization. **D. Chen:** Writing – review & editing, Software. **S. Corradetti:** Writing – review & editing, Supervision. **M. Lunardon:** Writing – review & editing, Supervision. **E. Mariotti:** Writing – review & editing, Supervision. **E. Reniero:** Software, Methodology, Investigation, Data curation. **D. Serafini:** Writing – review & editing, Software. **G.S. Valli:** Writing – original draft, Software, Methodology, Investigation. **L. Zangrando:** Writing – review & editing, Software. **A. Zenoni:** Writing – review & editing, Supervision. **A. Andrighetto:** Supervision, Resources, Project administration, Funding acquisition.

Declaration of competing interest

The authors declare that they have no known competing financial interests or personal relationships that could have appeared to influence the work reported in this paper.

Acknowledgments

This research was carried out in the framework of the ADMIRAL experiment of the National Scientific Committee 5 of INFN, Italy. The authors thank the members of the collaboration.

Data availability

Data will be made available on request.

References

Agostinelli, S., Allison, J., Amako, K., Apostolakis, J., Araujo, H., Arce, P., Asai, M., Axen, D., Banerjee, S., Barrand, G., et al., 2003. GEANT4a simulation toolkit. Nucl. Instruments Methods Phys. Res. Sect. A: Accel. Spectrometers, Detect. Assoc. Equip. 506 (3), 250–303. http://dx.doi.org/10.1016/S0168-9002(03)01368-8.

Allison, J., Amako, K., Apostolakis, J., Araujo, H., Arce Dubois, P., Asai, M., Barrand, G., Capra, R., Chauvie, S., Chytracek, R., Cirrone, G., et al., 2006. Geant4 developments and applications. IEEE Trans. Nucl. Sci. 53 (1), 270–278. http://dx.doi.org/10.1109/TNS.2006.869826.

Allison, J., Amako, K., Apostolakis, J., Arce, P., Asai, M., Aso, T., Bagli, E., Bagulya, A., Banerjee, S., Barrand, G., Beck, B., et al., 2016. Recent developments in GEANT4. Nucl. Instruments Methods Phys. Res. Sect. A: Accel. Spectrometers, Detect. Assoc. Equip. 835, 186–225. http://dx.doi.org/10.1016/j.nima.2016.06.125.

Andrighetto, A., Centofante, L., Gramegna, F., Monetti, A., Ballan, M., Zenoni, A., Corradetti, S., Lilli, G., Manzolaro, M., Marchi, T., Arzenton, A., Khwairakpam, O., Scarpa, D., Donzella, A., Mariotti, E., Meneghetti, G., Colombo, P., Biasetto, L., Oboe, R., Lunardon, M., Rifuggiato, D., 2023. Low energy radioactive ion beams at SPES for nuclear physics and medical applications. Nucl. Instruments Methods Phys. Res. Sect. B: Beam Interactions Mater. Atoms 541, 236–239. http://dx.doi.org/10.1016/j.nimb.2023.05.044.

Andrighetto, A., Tosato, M., Ballan, M., Corradetti, S., Borgna, F., Di Marco, V., Marzaro, G., Realdon, N., 2019. The ISOLPHARM project: ISOL-based production of radionuclides for medical applications. J. Radioanal. Nucl. Chem. 322 (1), 73–77. http://dx.doi.org/10.1007/s10967-019-06698-0.

Antoni, R., Bourgois, L., 2017. Evaluation of the new electron-transport algorithm in MCNP6.1 for the simulation of dose point kernel in water. Nucl. Instruments Methods Phys. Res. Sect. B: Beam Interactions Mater. Atoms 412, 102–108. http://dx.doi.org/10.1016/j.nimb.2017.09.026.

Arzenton, A., 2023. Radiobiological model for β^- emitter radiopharmaceutical therapy in dynamic cell cultures in the framework of the ISOLPHARM project. Il Nuovo Cimento C 46 (72), http://dx.doi.org/10.1393/ncc/i2023-23072-3.

Arzenton, A., 2024. Towards ^{111}Ag as a Medical Radionuclide: from Production and Laser Photo-Ionisation to Cell Dosimetry and Radiation Biophysics in the Context of the ISOLPHARM Project (Ph.D. thesis). Università degli Studi di Siena, URL https://usiena-air.unisi.it/handle/11365/1277135.

Ballan, M., Tosato, M., Verona, M., Caeran, M., Borgna, F., Vettorato, E., Corradetti, S., Zangrando, L., Sgaravatto, M., Verlato, M., et al., 2020. Preliminary evaluation of the production of non-carrier added ^{111}Ag as core of a therapeutic radiopharmaceutical in the framework of ISOLPHARM_Ag experiment. Appl. Radiat. Isot. 164, 109258. http://dx.doi.org/10.1016/j.apradiso.2020.109258.

Ballan, M., Vettorato, E., Morselli, L., Tosato, M., Nardella, S., Borgna, F., Corradetti, S., Monetti, A., Lunardon, M., Zenoni, A., Di Marco, V., Realdon, N., Andrighetto, A., 2021. Development of implantation substrates for the collection of radionuclides of medical interest produced via ISOL technique at INFN-LNL. Appl. Radiat. Isot. 175, 109795. http://dx.doi.org/10.1016/j.apradiso.2021.109795.

Bolch, W.E., Eckerman, K.F., Sgouros, G., Thomas, S.R., 2009. MIRD Pamphlet No. 21: A Generalized Schema for Radiopharmaceutical Dosimetry—Standardization of Nomenclature. J. Nucl. Med. 50 (3), 477–484. http://dx.doi.org/10.2967/jnumed.108.056036.

Brosch-Lenz, J., Delker, A., Völter, F., Unterrainer, L.M., Kaiser, L., Bartenstein, P., Ziegler, S., Rahmim, A., Uribe, C., Böning, G., 2023. Toward single-time-point image-based dosimetry of ^{177}Lu-PSMA-617 therapy. J. Nucl. Med. 64 (5), 767–774. http://dx.doi.org/10.2967/jnumed.122.264594.

Cai, Z., Kwon, Y.L., Reilly, R.M., 2017. Monte Carlo N-Particle (MCNP) modeling of the cellular dosimetry of ^{64}Cu: Comparison with MIRDcell S values and implications for studies of its cytotoxic effects. J. Nucl. Med. 58 (2), 339–345. http://dx.doi.org/10.2967/jnumed.116.175695.

Centofante, L., Donzella, A., Zenoni, A., Ferrari, M., Ballan, M., Corradetti, S., DAgostini, F., Lilli, G., Manzolaro, M., Monetti, A., Morselli, L., Scarpa, D., Andrighetto, A., 2021. Study of the radioactive contamination of the ion source complex in the Selective Production of Exotic Species (SPES) facility. Rev. Sci. Instrum. 92 (5), 053304. http://dx.doi.org/10.1063/5.0045063.

Corradetti, S., Andrighetto, A., 2020. The ISOLPHARM project: Production of high specific activity medical radioisotopes at SPES. Nucl. Phys. News 30 (4), 33–36. http://dx.doi.org/10.1080/10619127.2020.1752100.

Corradetti, S., Manzolaro, M., Carturan, S., Ballan, M., Centofante, L., Lilli, G., Monetti, A., Morselli, L., Scarpa, D., Donzella, A., Zenoni, A., Andrighetto, A., 2021. The SPES target production and characterization. Nucl. Instruments Methods Phys. Res. Sect. B: Beam Interactions Mater. Atoms 488, 12–22. http://dx.doi.org/10.1016/j.nimb.2020.12.003.

Denis-Bacelar, A.M., Chittenden, S.J., Dearnaley, D.P., Divoli, A., O'Sullivan, J.M., McCready, V.R., Johnson, B., Du, Y., Flux, G.D., 2017. Phase I/II trials of ^{186}Re-HEDP in metastatic castration-resistant prostate cancer: post-hoc analysis of the impact of administered activity and dosimetry on survival. Eur. J. Nucl. Med. Mol. Imaging 44 (4), 620–629. http://dx.doi.org/10.1007/s00259-016-3543-x.

Doctor, A., Seifert, V., Ullrich, M., Hauser, S., Pietzsch, J., 2020. Three-dimensional cell culture systems in radiopharmaceutical cancer research. Cancers 12 (10), http://dx.doi.org/10.3390/cancers12102765.

Endo, A., Yamaguchi, Y., Eckerman, K.F., 2005. Nuclear decay data for dosimetry calculation. Revised data of ICRP Publication 38.

Goorley, T., James, M., Booth, T., Brown, F., Bull, J., Cox, L., Durkee, J., Elson, J., Fensin, M., Forster, R., Hendricks, J., Hughes, H., Jonns, R., Kiedrowski, B., Martz, R., Mashnik, S., Mckinney, G., Pelowitz, D., Prael, R., Zukaitis, T., 2013. Initial MCNP6 Release Overview - MCNP6 Version 1.0. Tech. rep., Los Alamos National Laboratory, http://dx.doi.org/10.2172/1086758.

Grady Hughes, H., 2014. Enhanced electron-photon transport in MCNP6. In: Joint International Conference on Supercomputing in Nuclear Applications + Monte Carlo, vol. 2013, p. 03105. http://dx.doi.org/10.1051/snamc/201403105.

Hirayama, H., Namito, Y., Bielajew, A.F., Wilderman, S.J., Nelson, W.R., 2005. The EGS5 Code System. Tech. rep., Stanford Linear Accelerator Center, Stanford University, URL https://inspirehep.net/literature/701722.

Incerti, S., Baldacchino, G., Bernal, M., Capra, R., Champion, C., Francis, Z., Guèye, P., Mantero, A., Mascialino, B., Moretto, P., Nieminen, P., Villagrasa, C., Zacharatou, C., 2010. The Geant4-DNA project. Int. J. Model. Simul. Sci. Comput. 01 (02), 157–178. http://dx.doi.org/10.1142/S1793962310000122.

International Atomic Energy Agency (IAEA), 2025. IAEA Nuclear Data Services. https://www-nds.iaea.org.

Katugampola, S., Wang, J., Rosen, A., Howell, R.W., 2022. MIRD Pamphlet No. 27: MIRDcell V3, a revised software tool for multicellular dosimetry and bioeffect modeling. J. Nucl. Med. 63 (9), 1441–1449. http://dx.doi.org/10.2967/jnumed.121.263253.

Leso, A., 2023. Study of DNA Damage by Beta Radiation Using Geant4-DNA in the Context of the ISOLPHARM Project (M.S. thesis). Università degli Studi di Padova, URL https://thesis.unipd.it/handle/20.500.12608/51895.

Lilli, G., Centofante, L., Manzolaro, M., Monetti, A., Oboe, R., Andrighetto, A., 2023. Remote handling systems for the Selective Production of Exotic Species (SPES) facility. Nucl. Eng. Technol. 55 (1), 378–390. http://dx.doi.org/10.1016/j.net.2022.08.034.

Monetti, A., Andrighetto, A., Petrovich, C., Manzolaro, M., Corradetti, S., Scarpa, D., Rossetto, F., Dominguez, F.M., Vasquez, J., Rossignoli, M., Calderolla, M., Silingardi, R., Mozzi, A., Borgna, F., Vivian, G., Boratto, E., Ballan, M., Prete, G., Meneghetti, G., 2015. The RIB production target for the SPES project. Eur. Phys. J. A 51 (10), http://dx.doi.org/10.1140/epja/i2015-15128-6.

Monetti, A., Donzella, A., Ballan, M., Centofante, L., Corradetti, S., Ferrari, M., Lilli, G., Manzolaro, M., Marchi, T., Scarpa, D., Zangrando, L., Zenoni, A., Andrighetto, A., 2024. Study of the radionuclide deposition in the radioactive ion line of the Selective Production of Exotic Species (SPES) facility. Appl. Radiat. Isot. 204, 111121. http://dx.doi.org/10.1016/j.apradiso.2023.111121.

National Institute of Standards and Technology (NIST), 2025. Stopping Power and Range Tables for Electrons. https://physics.nist.gov/PhysRefData/Star/Text/ESTAR.html.

Reniero, E., 2023. Cellular Dosimetry using Geant4 in the Context of the ISOLPHARM Project (M.S. thesis). Università degli Studi di Padova, URL https://thesis.unipd.it/handle/20.500.12608/51905.

Sakata, D., Belov, O., Bordage, M.-C., Emfietzoglou, D., Guatelli, S., Inaniwa, T., Ivanchenko, V., Karamitros, M., Kyriakou, I., Lampe, N., Petrovic, I., Ristic-Fira, A., Shin, W.-G., Incerti, S., 2020. Fully integrated Monte Carlo simulation for evaluating radiation induced DNA damage and subsequent repair using Geant4-DNA. Sci. Rep. 10 (20788), http://dx.doi.org/10.1038/s41598-020-75982-x.

dos Santos Augusto, R.M., Buehler, L., Lawson, Z., Marzari, S., Stachura, M., Stora, T., collaboration, C.-M., et al., 2014. CERN-MEDICIS (medical isotopes collected from ISOLDE): a new facility. Appl. Sci. 4 (2), 265–281. http://dx.doi.org/10.3390/app4020265.

Sato, T., Iwamoto, Y., Hashimoto, S., Ogawa, T., Furuta, T., Abe, S.-I., Kai, T., Matsuya, Y., Matsuda, N., Hirata, Y., Sekikawa, T., Yao, L., Tsai, P.-E., Ratliff, H.N., Iwase, H., Sakaki, Y., Sugihara, K., Shigyo, N., Sihver, L., Niita, K., 2024. Recent improvements of the particle and heavy ion transport code system PHITS version 3.33. J. Nucl. Sci. Technol. 61 (1), 127–135. http://dx.doi.org/10.1080/00223131.2023.2275736.

Schaart, D.R., Jansen, J.T.M., Zoetelief, J., de Leege, P.F.A., 2002. A comparison of MCNP4C electron transport with ITS 3.0 and experiment at incident energies between 100 keV and 20 MeV: influence of voxel size, substeps and energy indexing algorithm. Phys. Med. Biol. 7 (47), 1459–1484. http://dx.doi.org/10.1088/0031-9155/47/9/303.

Serafini, D., Zancopè, N., Pavone, A.M., Benfante, V., Arzenton, A., Russo, V., Ballan, M., Morselli, L., Cammarata, F.P., Comelli, A., et al., 2025. ^{111}Ag phantom images with Cerenkov Luminescence Imaging and digital autoradiography within the ISOLPHARM project. Appl. Radiat. Isot. 215, 111562. http://dx.doi.org/10.1016/j.apradiso.2024.111562.

Shin, W.-G., Sakata, D., Lampe, N., Belov, O., Tran, N.H., Petrovic, I., Ristic-Fira, A., Dordevic, M., Bernal, M.A., Bordage, M.-C., Francis, Z., Kyriakou, I., Perrot, Y., Sasaki, T., Villagrasa, C., Guatelli, S., Breton, V., Emfietzoglou, D., Incerti, S., 2021. A Geant4-DNA Evaluation of Radiation-Induced DNA Damage on a Human Fibroblast. Cancers 13 (19), http://dx.doi.org/10.3390/cancers13194940.

Srivastava, S.C., Mausner, L.F., 2014. Therapeutic Nuclear Medicine. In: Ch. Therapeutic Radionuclides: Production, Physical Characteristics, and Applications, Springer Berlin Heidelberg, Berlin, Heidelberg, pp. 11–50. http://dx.doi.org/10.1007/174_2012_782.

Sun, Q., Li, J., Ding, Z., Liu, Z., 2023. Radiopharmaceuticals heat anti-tumor immunity. Theranostics 13 (2), 767–786. http://dx.doi.org/10.7150/thno.79806.

Tosato, M., Asti, M., 2023. Lights and shadows on the sourcing of silver radioisotopes for targeted imaging and therapy of cancer: Production routes and separation methods. Pharmaceuticals 16 (7), http://dx.doi.org/10.3390/ph16070929.

Tosato, M., Gandini, A., Happel, S., Bas, M., Donzella, A., Zenoni, A., Salvini, A., Andrighetto, A., Marco, V.D., Asti, M., 2023. Chromatographic separation of silver-111 from neutron-irradiated palladium target: toward direct labeling of radiotracers. EJNMMI Radiopharm. Chem. 8 (43), http://dx.doi.org/10.1186/s41181-023-00232-0.

Vaziri, B., Wu, H., Dhawan, A.P., Du, P., Howell, R.W., 2014. MIRD Pamphlet No. 25: MIRDcell V2.0 software tool for dosimetric analysis of biologic response of multicellular populations. J. Nucl. Med. 55 (9), 1557–1564. http://dx.doi.org/10.2967/jnumed.113.131037.